Simulation of satellite infrared radiances for convective-scale data assimilation over the Mediterranean

Fanny Duffourg, Véronique Ducrocq, Nadia Fourrié, Geneviève Jaubert, Vincent Guidard

▶ **To cite this version:**

HAL Id: meteo-00564288

https://meteofrance.hal.science/meteo-00564288

Simulation of satellite infrared radiances for convective-scale data assimilation over the Mediterranean

Fanny Duffourg,[1] Véronique Ducrocq,[1] Nadia Fourrié,[2] Geneviève Jaubert,[1] and Vincent Guidard[2]

[1]   This paper focuses on the simulation of satellite infrared passive observations for their assimilation in high horizontal resolution (2.5 km) numerical weather prediction systems. In order to better represent the sensitivity of the satellite measurement to the whole atmosphere within its footprint, new observation operators are designed. They aggregate the model information contained within the satellite field of view. The different observation operators are evaluated for the simulation of Infrared Atmospheric Sounding Interferometer (IASI) and Atmospheric Infrared Sounder (AIRS) observations over a whole month. The new observation operators are found to improve the simulation of water vapor channels and to have neutral to slightly negative impact for temperature channels. For most channels, the standard deviation of the observation minus guess departures is reduced. The modifications of the simulations are substantial for water vapor channels for which the weighting functions peak at pressures greater than 340 hPa for IASI and between 340 hPa and 800 hPa for AIRS. The most important ones appear where fine-scale humidity gradients occur in dry sounded layers. The new observation operators improve the simulation of IASI and AIRS observations by filtering out these fine-scale patterns that are not detected by the instruments. With improvements in observations minus guess reaching 2 K, the new observation operators may avoid the rejection of some observations by quality control procedures during the assimilation process. Single observation assimilation experiments are then carried out using the different observation operators. They show that even large modifications in the observation simulation have almost no impact on the final analysis.

1.   Introduction

[2]   A number of meteorological centers have recently developed convective-scale numerical weather prediction (NWP) systems with the specific aim of improving the forecasting of high-impact weather events. Their kilometer-sized grid mesh, nonhydrostatic equations and improved microphysics parameterizations enable atmospheric deep convection to be resolved explicitly. The representation of the precipitating systems is thus significantly improved. Case studies focusing on Mediterranean heavy rainfall events have shown significant forecast improvements using nonhydrostatic convective-scale research models [*Ducrocq et al.*, 2002]. However, these studies have also pointed out the necessity to improve, in particular, the representation in the initial conditions of the moisture field as Mediterranean heavy rainfall simulations are very sensitive to the mesoscale structure of this field that is highly variable in space and time. A better ability to simulate the dynamical and physical processes at fine scale is not always sufficient to prevent bad forecasts. If some mesoscale key mechanisms are missing in the initial conditions, the model fails to reproduce the precipitating systems.

[3]   Convective-scale assimilation of observations is a way to improve the initial conditions of kilometer-scale models. Such improvement over the sea is of particular importance because some Mediterranean heavy rainfall is triggered off shore [*Nuissier et al.*, 2008]. Over the sea, satellite data are practically the only routinely available observations. The new Infrared Atmospheric Sounding Interferometer (IASI) [*Cayla*, 2001; *Chalon et al.*, 2001] and Atmospheric Infra-Red Sounder (AIRS) [*Pagano et al.*, 2002; *Aumann et al.*, 2003] now offer high-resolution and accurate information

[1]Groupe de Météorologie de Moyenne Echelle, Centre National de Recherches Météorologiques, Groupe d'étude de l'Atmosphère Météorologique, Météo-France, Centre Nationale de la Recherche Scientifique, Toulouse, France.

[2]Groupe de Modélisation pour l'Assimilation et la Prévision, Centre National de Recherches Météorologiques, Groupe d'étude de l'Atmosphère Météorologique, Météo-France, Centre Nationale de la Recherche Scientifique, Toulouse, France.

on temperature and humidity. IASI sounds the atmosphere with a horizontal resolution of 12 km at nadir. The accuracy of its measurements is expected to be better than 1 K for temperature retrievals and 10% below 500 hPa for relative humidity retrievals with a vertical resolution finer than 1 km [*Diebel et al.*, 1996]. The initial model analysis may therefore benefit from the assimilation of such new information over the sea.

[4] However, the assimilation of satellite data in a convective-scale data assimilation system is not straightforward. New problems arise, in particular because of the scale difference between model and satellite measurements: the model mesh is about 1 order smaller than any satellite observation spot. This problem is frequently encountered in hydrological applications when the satellite soil moisture data need to be retrieved at the finer scale of the hydrological model. In the past, several studies have addressed this issue, proposing that the satellite measurements should be disaggregated at the model scale by characterizing subpixel variability [*Reichle et al.*, 2001; *Kim and Barros*, 2002; *Merlin et al.*, 2005]. This approach cannot, however, be applied when the satellite measurements are directly assimilated without any previous retrieval. The variational data assimilation methods of the NWP systems which assimilate the satellite radiances directly, require indeed equivalent observations simulated from the values provided by the model to be compared with the real observations. For such simulations, model information from the different grid columns contained within the satellite field of view has to be aggregated. This issue has already been investigated by *Kleespies* [2009] for the assimilation of microwave sounder measurements: surface model parameters are aggregated to improve the simulation in case of nonuniform scenes. The aim of our study is to address this question by gathering atmospheric model information and focusing on the accurate, high-resolution IASI and AIRS infrared sounders.

[5] More precisely, the main purpose of this paper is to evaluate different methods for aggregating atmospheric model information contained in the satellite field of view to simulate IASI and AIRS observations. This issue is examined more specifically for the newly developed convective-scale 3D-Var data assimilation system of Météo-France called AROME (Application of Research to Operations at MEsoscale) and for the Mediterranean. We follow the ideas of the studies of *Brenot et al.* [2006], which evaluated the sensitivity to various formulations of Global Positioning System (GPS) zenith delay simulations, and *Caumont et al.* [2006] and *Caumont and Ducrocq* [2008] for the effect of how radar reflectivity and Doppler wind simulations, respectively, were formulated. Different ways of aggregating the model information within a IASI or AIRS spot are developed. They are described in section 2 together with the AROME system and the IASI and AIRS measurements. Section 3 evaluates the maximum differences between the various methods of aggregation for the simulation of IASI and AIRS brightness temperatures. The different simulations are then compared with real observations in section 4. Lastly, section 5 discusses the impact on the AROME analysis of the different methods for computing the model equivalent radiances by performing single observation

assimilation experiments. Conclusions and outlooks follow in section 6.

2. Description of the Assimilation of Satellite Infrared Radiances in AROME

2.1. AROME 3D-Var

[6] AROME [*Ducrocq et al.*, 2005; *Yan et al.*, 2009] is a Limited Area Model (LAM) with a 2.5 km grid covering the territory of France including the northwestern part of the Mediterranean Sea (5.2°W to 11.2°E, 40.5°N to 51.7°N). It is coupled hourly with the ALADIN (Aire Limitée, Adaptation dynamique, Développement InterNational) forecast [*Radnóti et al.*, 1995] on its lateral boundaries. The 41 unequally spaced vertical levels cover the troposphere (with 30 levels) and, more loosely, the stratosphere up to about 1 hPa. AROME is a three-dimensional nonhydrostatic model, the dynamics of which is based on the ALADIN nonhydrostatic equations [*Bubnová et al.*, 1995]. The prognostic equations of the six water species (water vapor, cloud water, rain water, cloud ice crystals, snow and graupel) as well as the physical parameterizations are shared with the nonhydrostatic Meso-NH model [*Lafore et al.*, 1998].

[7] AROME has its own 3D-Var data assimilation system [*Brousseau et al.*, 2008], based on that of ALADIN-FRANCE [*Fischer et al.*, 2005; *Guidard et al.*, 2006]. As such, it adopts the incremental formulation originally introduced in the ARPEGE/IFS (Action Recherche Petite Echelle Grande Echelle/Integrated Forecast System) global data assimilation system [*Courtier et al.*, 1994]. The AROME background error covariances are based on the same multivariate formulation as in ALADIN-FRANCE [*Berre*, 2000]. The design of the observation-error covariance matrix assumes that there are no observation-error correlations.

[8] The operational AROME 3D-Var data assimilation system uses a 3 h forward intermittent cycle: observations within a ±1 h 30 min assimilation window are used to perform the analysis from which a 3 h forecast is obtained to serve as a first guess for the next cycle. The two wind components, temperature, specific humidity and surface pressure are analyzed. Other model fields are cycled from the previous AROME guess. All conventional observations are assimilated (surface observations from land stations and ships, vertical soundings from radiosondes and pilot balloons, buoy and aircraft measurements), together with wind profilers, winds from Atmospheric Motion Vectors (AMV) and scatterometers, Doppler winds from radars, satellite radiances (such as IASI and AIRS measurements) as well as ground-based GPS measurements. Satellite radiances (or the corresponding brightness temperatures) are directly assimilated, using an observation operator that simulates the model-equivalent radiances. This observation operator is described in section 2.3. The differences between real and model-equivalent observations are bias-corrected with an adaptive variational method [*Dee*, 2004; *Auligné et al.*, 2007] before entering in the minimization of the variational cost function for the computation of the analysis.

2.2. IASI and AIRS Measurements

[9] IASI and AIRS are hyperspectral infrared passive nadir scanning radiometers, onboard the European MetOp and the

Table 1. IASI and AIRS Geometrical Characteristics[a]

Instrument	Angular FOV	Nadir Spot Size	Maximum Scan Angle	Maximum Spot Size
IASI	1.1°	12 km	48.3°	38 km × 20 km
AIRS	0.825°	13.5 km	49.5°	40 km × 22 km

[a]Nadir spot size corresponds to the diameter of the circular spot, and maximum spot size corresponds to the major and minor axes of the ellipsoidal spot. FOV stands for field of view.

American Aqua polar orbiting satellites, respectively. They measure the radiation coming out of the atmosphere on thousands of channels in the infrared spectrum (8461 for IASI and 2378 for AIRS). The measured outgoing radiation results from all the radiative emissions of each layer of the atmosphere and the surface, weakened by the atmospheric absorption (if the atmospheric diffusion is neglected which is realistic in clear-sky conditions). The measured radiances can thus be expressed by the following radiative transfer equation:

$$L_\lambda(\text{sat}) = \varepsilon_\lambda(\text{surf})B_\lambda(T_s)\tau_\lambda(\text{surf}) + \int_{z_{\text{surf}}}^{z_{\text{sat}}} \varepsilon_\lambda B_\lambda(T(z))\tau_\lambda(z)\text{d}z,$$
(1)

where λ is the wavelength of the considered radiation, L_λ is the radiance in this wavelength, $\varepsilon_\lambda(\text{surf})$ the surface emissivity, ε_λ the atmospheric emissivity, $B_\lambda(T)$ the black body radiance, T_s the surface temperature, z_{surf} the altitude of the surface, z_{sat} the altitude of the satellite and $\tau_\lambda(z)$ the transmission (the proportion of the radiation which has not been absorbed when passing through the atmospheric layer between the altitude z and the satellite). Radiation absorption and emission in the different layers of the atmosphere are sensitive to the meteorological conditions (humidity and temperature). The measured radiance is therefore strongly linked with the meteorological parameters in some specific highly sensitive zones of the atmosphere depending on the wavelength. For each channel, the vertical layers contributing to the radiances are represented by weighting functions.

[10] IASI and AIRS spectra can be divided into three major bands: (1) from 645 cm^{-1} to 1210 cm^{-1} (wavelength from about 8.25 μm to about 15.5 μm): CO_2 band mainly sensitive to temperature, named Temperature Long Wave band (TLW); (2) from 1210 cm^{-1} to 2040 cm^{-1} (wavelength from about 4.9 μm to about 8.25 μm): band mainly sensitive to humidity, named Water Vapour band (WV); and (3) from 2040 cm^{-1} to 2700 cm^{-1} (wavelength from about 3.7 μm to about 4.9 μm): band mainly sensitive to temperature, named Temperature Short Wave band (TSW).

[11] A subset of IASI and AIRS channels was selected for this study. Within the classical sets of 314 IASI and 324 AIRS channels defined for operational NWP applications ([*Collard*, 2007] for IASI, [*Susskind et al.*, 2003] for AIRS), only the channels assimilated operationally at ECMWF in 2007 were kept. Although very few data from IASI WV and non-Sun-sensitive TSW channels are currently assimilated by operational meteorological centers, these channels were all kept in this study to prepare for their future use. Within these subsets, we selected only the channels sounding below the tropopause as the vertical resolution within the stratosphere in AROME is not sufficient to simulate the strato-

spheric sounding channels correctly. This selection led to a subset of 120 AIRS and 163 IASI channels.

[12] IASI and AIRS are nadir-viewing sounders: they scan the atmosphere for different look positions along a plane which is perpendicular to the satellite orbit track. When looking at an off-nadir position, the atmosphere is scanned along a slanted line of sight. Table 1 gives the maximum angle formed between the line of sight and the nadir direction. As IASI and AIRS fields of view are 0.825° and 1.1°, respectively, the horizontal resolution of their measurements varies with the scan angle. The minimum (at nadir) and maximum (at swath edge) sizes of the satellite observation spot are given in Table 1 and range from 12 km to 40 km along the major axis of the ellipsoidal spot.

[13] The data used in this study were level 1c products provided for operational purposes by EUMETSAT (EUropean organisation for the exploitation of METeorological SATellites) for IASI and NESDIS (National Environmental Satellite Data and Information Service) for AIRS. The NESDIS AIRS product is available only for every ninth scan position.

2.3. IASI and AIRS Observation Operators

[14] The simulation of satellite brightness temperature from the model atmospheric profile is performed in two main steps by the observation operator. The first step forms a model column that represents the sounded atmosphere. The second step uses this model column to compute the simulated brightness temperature using a radiative transfer model. The brightness temperature calculation is performed with the Radiative Transfer for TOVS (RTTOV) model [*Saunders and Brunel*, 2005] which models the complex relationship linking the atmospheric profile with the radiances measured by satellite nadir scanning radiometers (as expressed by equation (1)). We used the version 8.5 of RTTOV with the default 43 levels. In our case, RTTOV was based on the line-by-line transmittance model GENLN2 [*Edwards*, 1992].

[15] In the operational AROME data assimilation system, the model column representing the sounded atmosphere is estimated at the center of the satellite observation spot by interpolating the four closest model columns surrounding this point. This procedure, called COL4 hereafter, comes from the previous larger-scale assimilation systems for which the model grid mesh is larger than the observation spot. However, with a 2.5 km horizontal resolution like the one used for AROME, a single IASI or AIRS observation spot covers more than 12 model grid points at nadir and about a hundred at swath edge. The instrument's point spread function is quasi-uniform over the spot (*Blumstein* [2005] for IASI and *Elliott et al.* [2006] for AIRS), so it is legitimate to consider that every model grid point in the spot contributes similarly to the measurement. The same weight for each grid point was thus used in the new aggregation methods developed in this study. Three new observation operators aggregating the model information contained within the satellite field of view were defined (Table 2 and Figure 1). In the observation operator called SPOT1 hereafter, the sounded atmosphere is represented by the mean of all the model columns located in the observation spot. This mean model column is then used to estimate the brightness temperature with RTTOV. For M12, the sounded atmosphere is estimated as the mean of the 12 model columns surrounding the center

Table 2. Characteristics of the Different Observation Operators

Operator	Method
COL4	four-point interpolation
M12	mean over 12 points before radiative transfer
SPOT1	mean over the spot before radiative transfer
SPOT2	mean over the spot after radiative transfer

of the observation spot. Finally, a more realistic observation operator averages the estimated brightness temperatures from each model column in the spot rather than averaging the model columns before the radiative transfer. This was found to be almost the same as averaging the radiances from each model column within the spot. This third observation operator, called SPOT2, requires much more computing time however, which is an important drawback for operational use.

3. Intercomparison of the Observation Operators

3.1. Methodology

[16] In this section, we examine what the maximum impact of a change in the observation operator may be on the simulation of IASI and AIRS brightness temperatures. For the whole month of September 2007, the four observation operators (Table 2) were applied to simulated observation spots centered on each grid point of every 3 h AROME analysis provided by a data assimilation cycle as described in section 2.1. Only clear simulated spots situated over the western Mediterranean Sea were considered. A simulated observation spot was clear if the mixing ratio of the total hydrometeors was less than 10^{-6} kg/kg over all the model columns included in the spot. The operational cloud detection system (the "cloud detect" software by *McNally and Watts* [2003]) could not be used here as no real observations were considered. Also, a simulated spot was defined as over the sea if, according to the model land-sea mask, the whole spot was entirely over sea. The observation operators were applied considering the maximum size of the observation spot (i.e., simulating swath edge measurements), in order to evaluate the maximum differences between the various observation operators.

[17] Mean biases and standard deviations for IASI and AIRS brightness temperature differences between the calculations with the various operators over the whole of September 2007 were computed using COL4 as the reference. The significance of the results was evaluated by comparison with the instrument noise, estimated in terms of Noise Equivalent Differential Temperature (NEDT). *Blumstein* [2007] gives the NEDT values for each IASI channel at the reference temperature of 280 K, and *Pagano et al.* [2002, 2003] give the values for AIRS at 250 K. With these reference values, NEDT was computed at the mean brightness temperature over the month for each channel, following *Chalon et al.* [2001]. It was verified that the variations of NEDT over the month remained within ±10% of the value computed with the monthly mean temperature (not shown).

3.2. Results Over the Month of September 2007

[18] For all the channels studied, Figure 2 shows the standard deviation over the whole month of September 2007 of the brightness temperature differences between calcula-

tions using the three new observation operators (M12, SPOT1 and SPOT2; see Table 2) and the current one (COL4), together with the NEDT. Figure 3 zooms in the WV channels.

[19] The standard deviations for SPOT1 and SPOT2 are remarkably close: the corresponding curves are almost superimposed. As expected, brightness temperature differences between SPOT1 or SPOT2 and COL4 are greater than differences between M12 and COL4 for most channels.

[20] For the three new observation operators, the standard deviation of the brightness temperature differences with COL4 is lower than the instrument noise for all TLW and TSW IASI and AIRS channels and also for the short-wave part of the IASI WV band (wave number between 1920 cm^{-1} and 2040 cm^{-1}). Substantial differences between SPOT1 (or SPOT2) and COL4 (i.e., larger than the NEDT) appear mainly for IASI and AIRS WV channels for which the weighting function peaks at pressures greater than 340 hPa for IASI, and between 340 hPa and 800 hPa for AIRS (wave number from 1210 to about 1455 cm^{-1} plus channel 3263, 1460.50 cm^{-1}, for IASI and from about 1315 to 1600 cm^{-1}, except three channels around 1550 cm^{-1} and channel 1449, 1330.98 cm^{-1}, for AIRS). These differences are smaller for AIRS channels with broad weighting functions (e.g., channel 1471, 1342.24 cm^{-1}). The differences between M12 and COL4 calculations are smaller; they remain substantial only for the low to middle troposphere (under 400 hPa) sounding channels with low NEDT (e.g., IASI channel 2889, 1367.00 cm^{-1}, and AIRS channel 1627, 1427.23 cm^{-1}).

[21] The impact of the new observation operators is larger on the simulation of WV channels because these channels are much more sensitive to atmospheric temperature and humidity than temperature channels. Figure 4 shows this difference in sensitivity for a IASI TLW channel and a IASI WV channel. It exhibits the Jacobians in temperature and specific humidity of both channels.
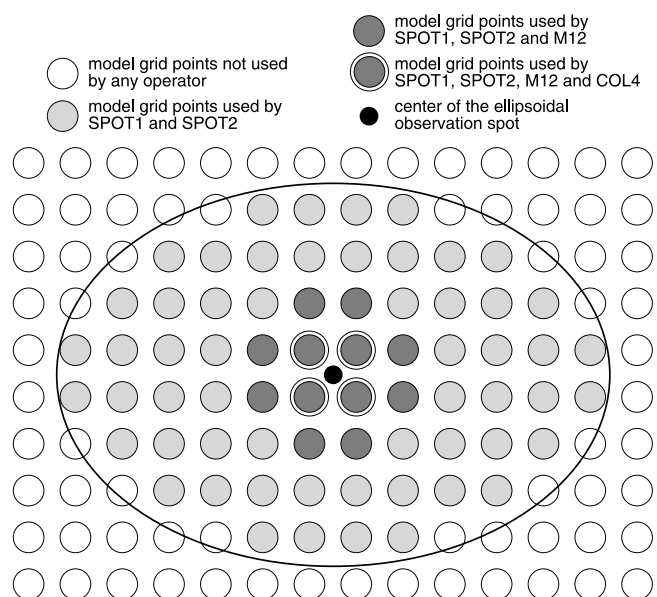

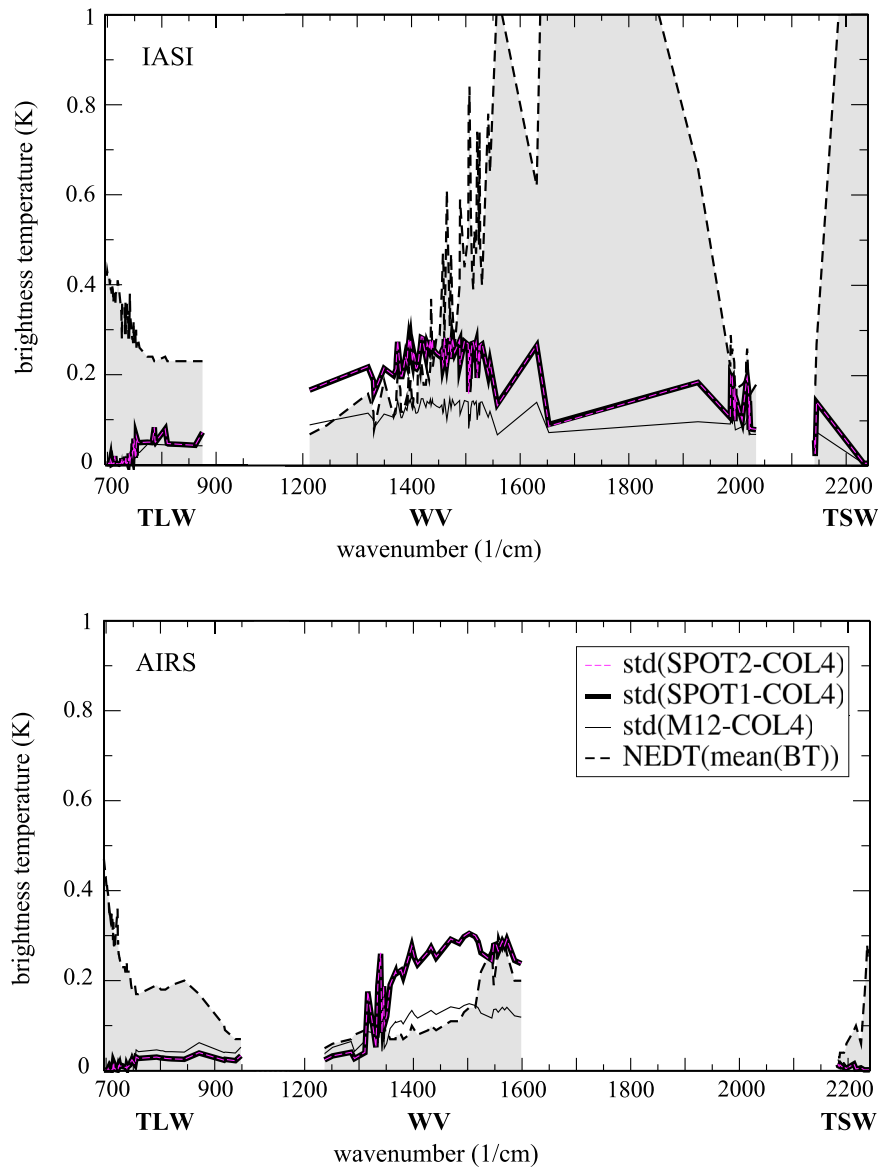**Figure 1.** The model grid points aggregated by the different observation operators.

Figure 2. Standard deviation (in K) of the brightness temperature (BT) differences between simulations with a new observation operator (M12 in thin solid black line and SPOT2 in thin dashed violet line plotted on top of SPOT1 in thick solid black line) and COL4 for all the IASI and AIRS channels studied, displayed according to increasing wave number along the abscissa. The instrument NEDT estimated for each channel at the monthly mean brightness temperature is represented by the dashed black line, with the area under this line colored in grey.

[22] For the three new observation operators, the average of the brightness temperature differences with COL4 is very close to 0 K for each channel: no new biases have been introduced.

[23] Figure 5 shows the standard deviation of the brightness temperature differences between SPOT2 and SPOT1. Its comparison with the instrument noise confirms that using a spot-averaging method closer to the measurement (SPOT2) does not bring results substantially different from averaging first the model information over the spot before computing the brightness temperature (SPOT1). The standard deviation of their differences is indeed lower than the NEDT for all the IASI and AIRS WV channels. Even

smaller differences between the two operators were found for IASI and AIRS TLW and TSW channels and for IASI channels of the short-wave part of the WV band (not shown).

[24] The histograms of the brightness temperature differences between SPOT1 or SPOT2 and COL4 for IASI WV channel 2919 and AIRS WV channel 1627 are displayed in Figure 6. Histograms for other WV channels (not shown) have a similar shape. They all show that the largest differences with COL4 are slightly weaker using SPOT2 rather than SPOT1. This is the main difference between calculations with SPOT1 and SPOT2 as both observation operators were globally in good agreement with each other for situa-
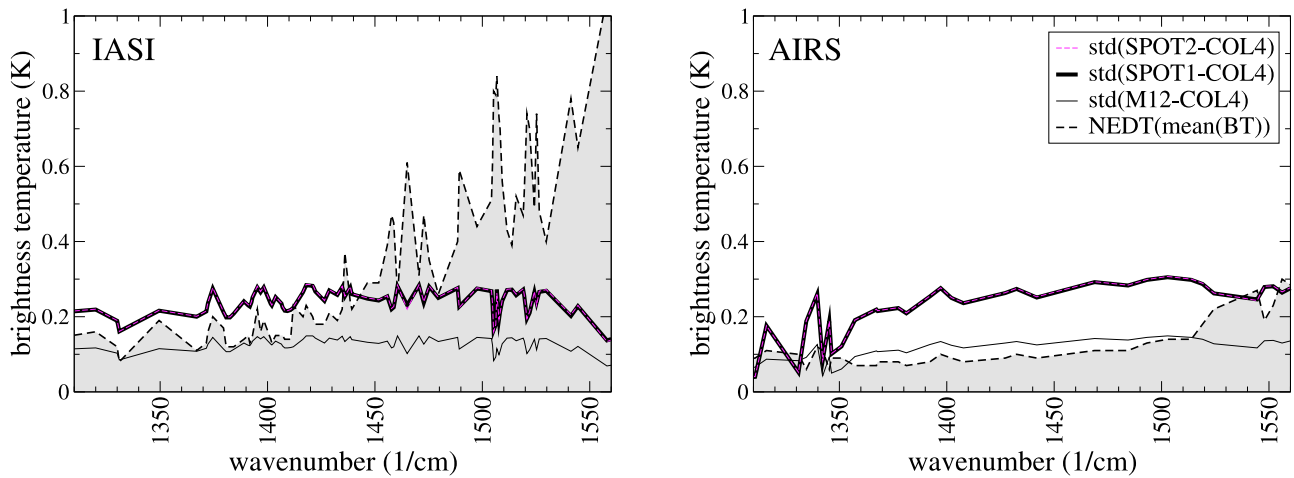
Figure 3. Zoom in on the WV channels of Figure 2.

tions where their simulations were closer to the COL4 calculations. This is not important enough to justify the use of a much more computing-time-consuming observation operator in an operational and real time context. In consequence, SPOT1 will be preferred.

[25] Finally, to assess the temporal variability of the brightness temperature differences between the various observation operators, the standard deviations of these differences were computed on each 3 h AROME analysis. Time series are shown on Figure 7 for some of the WV channels identified above as having substantial differences between SPOT1 and COL4 simulations: four IASI WV channels (2271 (1212.50 cm^{-1}), 2889 (1367.00 cm^{-1}), 2919

(1374.50 cm^{-1}) and 3244 (1455.75 cm^{-1})) and three AIRS WV channels (1455 (1334.60 cm^{-1}), 1627 (1427.23 cm^{-1}) and 1794 (1563.71 cm^{-1})). The corresponding weighting functions (Figures 7b and 7d) show that the part of the atmosphere sounded is quite different among the selected channels. The temporal variability of the brightness temperature differences between SPOT1 and COL4 is much greater than the instrument noise time variation. The amplitude of the instrument noise time variations ranges indeed from 0.015 K for the least variable channels, such as IASI channel 2271 and AIRS channel 1455, to 0.14 K or 0.19 K for the most variable ones, such as AIRS channel 1794 or IASI channel 3244 (not shown), whereas the var-
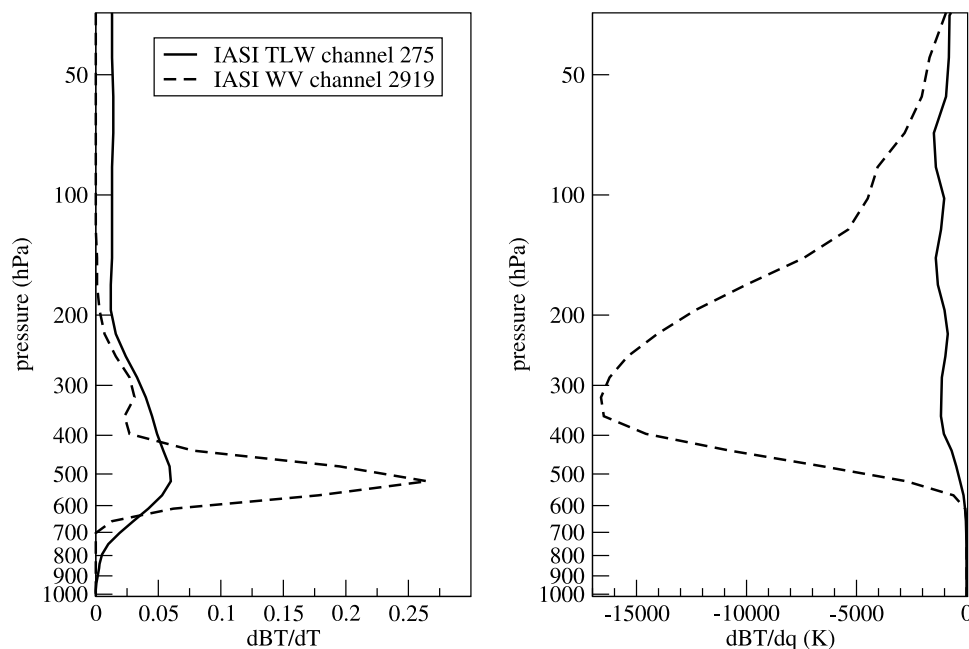

Figure 4. Jacobians in (left) temperature and (right) specific humidity for IASI TLW channel 275 (713.50 cm^{-1}) and IASI WV channel 2919 (1374.50 cm^{-1}), calculated for the observation of 2100 UTC, 6 September 2007, considered in section 5 (see Figure 12a for its location).
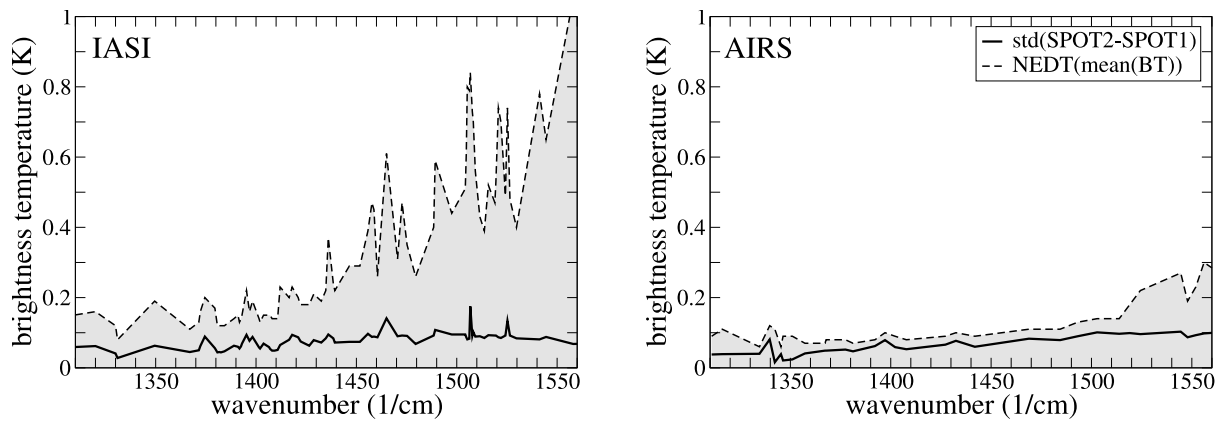
Figure 5. Same as Figure 3 but for brightness temperature differences between simulations with SPOT2 and SPOT1.

iations of the brightness temperature differences between SPOT1 and COL4 reach more than 0.4 K for the least variable channels and 1 K for the most variable ones (see Figure 7). The time variations are consistent among the different channels. The channels exhibit the largest differences for the same days (for instance 6, 16 or 24 September: the results for the 26 to 28 September period are not reliable as very few points were clear over the Mediterranean). Standard deviations as large as 0.5 to 1 K were obtained between SPOT1 and COL4 for these days for upper-level sounding channels.

3.3. Case Study: 24 September 2007

[26] As stated above, using SPOT1 instead of the current observation operator COL4 may substantially modify the simulated brightness temperatures of IASI and AIRS WV channels, especially for some specific days. Some particular fine-scale meteorological patterns present on these days can explain why averaging the model information over the whole spot leads to an estimation of the sounded atmosphere substantially different from that obtained using only four-point interpolation. We focus here on one of these situations,

on 24 September 2007 at 2100 UTC, in order to determine the reasons for such large differences in the simulation of brightness temperatures.

[27] Figure 8 shows the simulation, at this date, of IASI 2919 water vapor channel brightness temperatures with COL4, M12 and SPOT1 together with the model relative humidity at 7000 m where the IASI channel 2919 peaks. The largest differences between the observation operator calculations are found in an area of fine-scale elongated filaments of moisture in the atmospheric layers observed. The same fine-scale filament pattern is evidenced in COL4 simulations, whereas it is partially smoothed with M12 by the 12-point average. With SPOT1, the spot-average filters out the fine-scale gradients of a size smaller than the observation resolution. So we can conclude that, in areas where strong fine-scale humidity gradients occur, COL4 and, to a lesser extent, M12 simulate brightness temperature structures that cannot be measured by the satellite. This can result in large differences between observed and first-guess equivalent radiances, which will lead to rejection of the observations or to production of too large analysis incre-
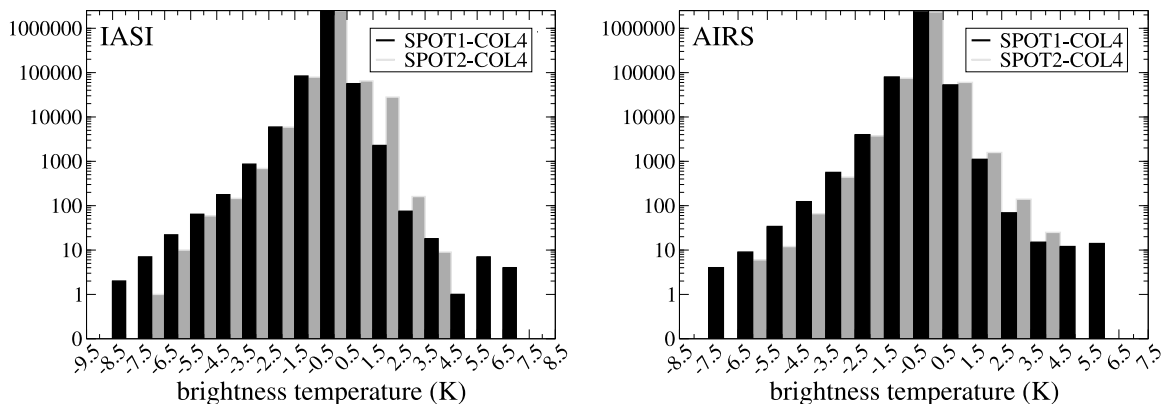

Figure 6. Histograms of the brightness temperature differences between simulations with SPOT1 and COL4 (black) and between simulations with SPOT2 and COL4 (grey) for IASI WV channel 2919 (1374.50 cm^{-1}) and AIRS WV channel 1627 (1427.23 cm^{-1}). The y axis is logarithmic.
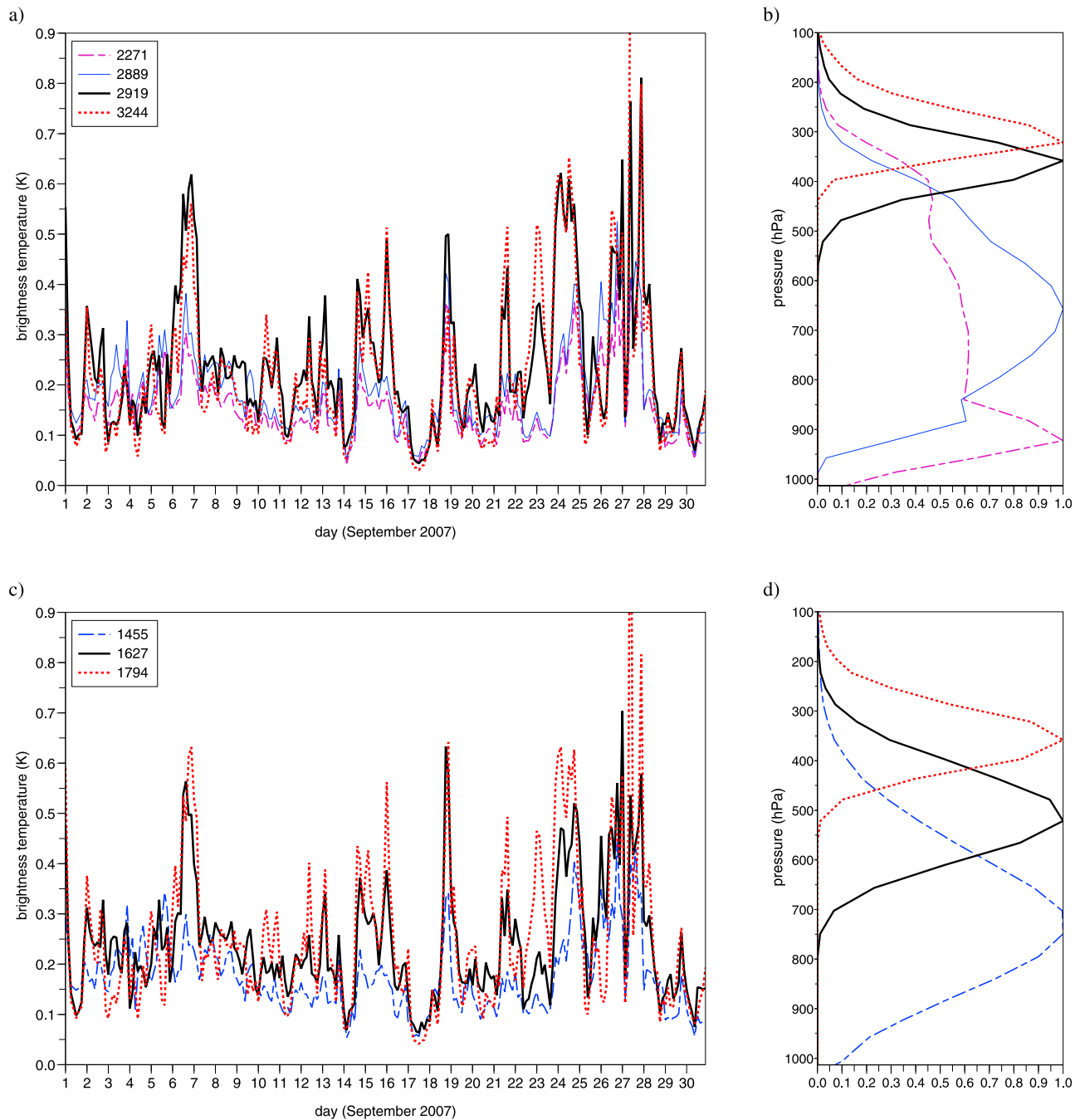
Figure 7. Time series over September 2007 of the standard deviation of the brightness temperature differences between simulations with SPOT1 and COL4 of (a) four IASI WV channels, 2271 (1212.50 cm^{-1}), 2889 (1367.00 cm^{-1}), 2919 (1374.50 cm^{-1}), and 3244 (1455.75 cm^{-1}), and (c) three AIRS WV channels, 1455 (1334.60 cm^{-1}), 1627 (1427.23 cm^{-1}), and 1794 (1563.71 cm^{-1}), in clear sky over western Mediterranean. The weighting functions of these channels (b) for IASI and (d) for AIRS were estimated with the U.S. Standard Atmosphere.

ments in the data assimilation process. Using SPOT1 might thus avoid these drawbacks.

[28] It is worth mentioning that the main brightness temperature differences between the three observation operators occur when very dry air conditions prevail. The other important differences encountered during September 2007 (situations identified on Figure 7) also arose in areas exhibiting spatial humidity variations in a very dry atmo-sphere. In such dry environment, moisture variations that are not particularly large in absolute terms become important relatively to the moisture content. Past studies such as those by *Berg et al.* [1999] for the High-resolution Infrared Radiation Sounder (HIRS) channel 12 and Special Sensor Microwave/Temperature 2 (SSM/T2) channel 2 or *Soden and Bretherton* [1996] for Geostationary Operational Environmental Satellites (GOES) channels also state that the
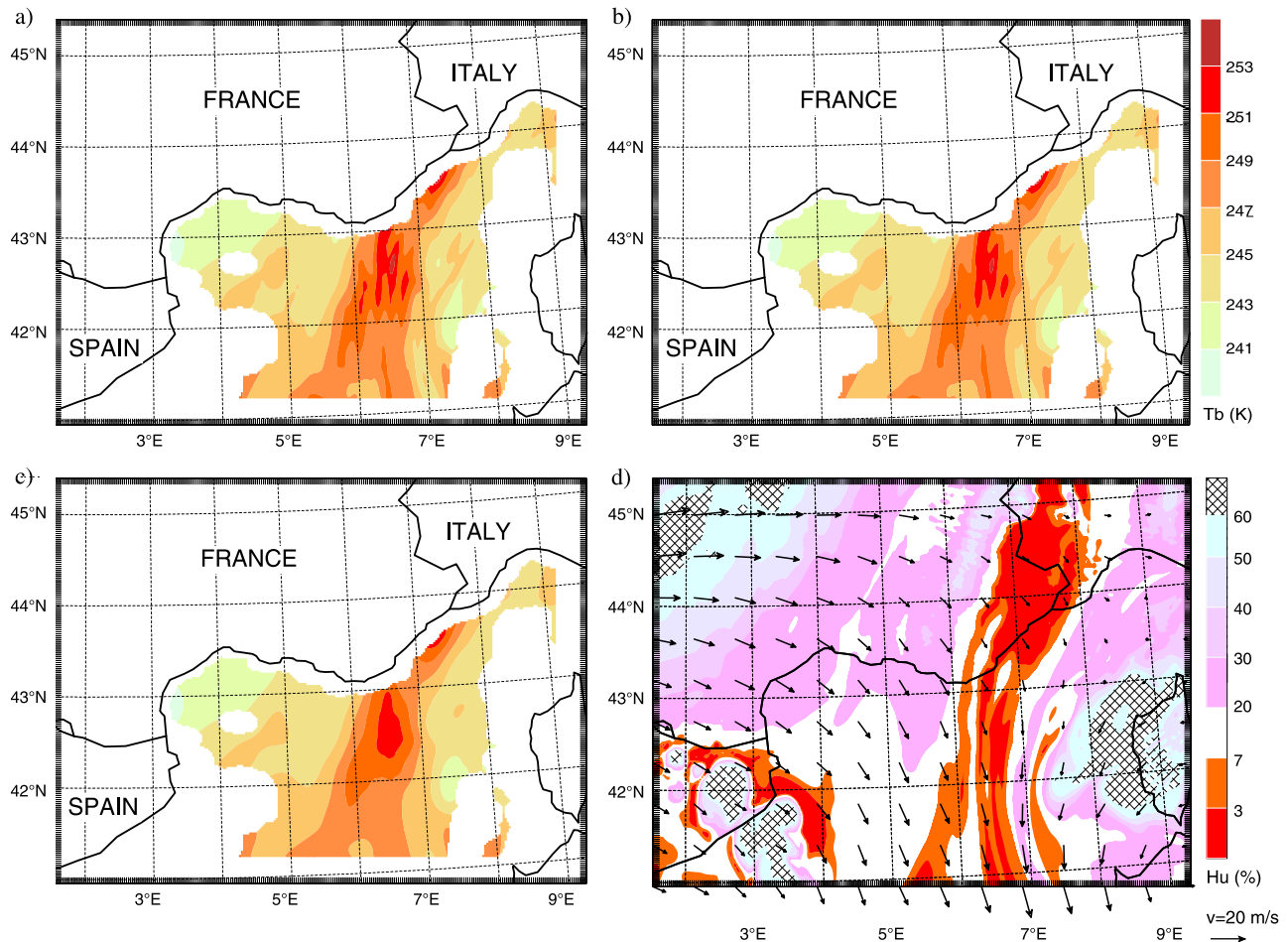
Figure 8. Simulation of IASI WV channel 2919 brightness temperature (in K, scale at the top right) at 2100 UTC, 24 September 2007 using (a) COL4, (b) M12, and (c) SPOT1; (d) 7 km ASL wind vector and relative humidity (in percent, scale at the bottom right). Observation operators are applied only over the sea and for cloud free areas. Wind arrows are drawn every 20 grid points with a scale in m/s given by the length of the arrow at the bottom right of Figure 8d.

sensitivity of the brightness temperature to atmospheric relative humidity increases with the dryness of the sounded air mass.

4. Comparison to the Observed Radiances

[29] So far, the impact of a change in the observation operator on the simulation of IASI and AIRS brightness temperature has proved substantial in the special case of a maximum scan angle and with specific meteorological conditions. This impact will now be assessed more generally for real observations in order to determine whether one observation operator provides model equivalent observations that are globally closer to the observations than another operator does.

[30] For this purpose, the screening stage of the 3 h AROME data assimilation cycle was performed throughout the month of September 2007. All clear IASI and AIRS observations situated over the Mediterranean Sea were thus simulated with COL4, M12 and SPOT1 from the 3 h AROME forecast which served as the first guess in the data assimilation cycle. An observation was considered to be over sea if, according to the

model land-sea mask, all the model grid points covered by the observation spot were over the sea. For each observation, the "cloud detect" software of *McNally and Watts* [2003], which is used for the operational data assimilation of satellite observations, was applied here to distinguish between clear and cloudy channels.

[31] The departures between the observations (without bias correction) and their simulations with the three observation operators were calculated in order to see if they decreased when the new observation operators were used. As only one AIRS observation out of nine was provided, there were too few clear AIRS observations over the Mediterranean Sea to compute significant statistics. The following therefore focuses only on IASI observations. The number of clear IASI observations used is of about a hundred for the near-surface channels, and ranges from about 500 for the channels sounding around 950 hPa to more than 5000 for the highest peaking channels (near-tropopause channels).

[32] Figure 9 shows the histograms of the differences between |obs − guess| obtained with SPOT1 or M12 and |obs − guess| obtained with COL4 for the IASI WV channel

a)

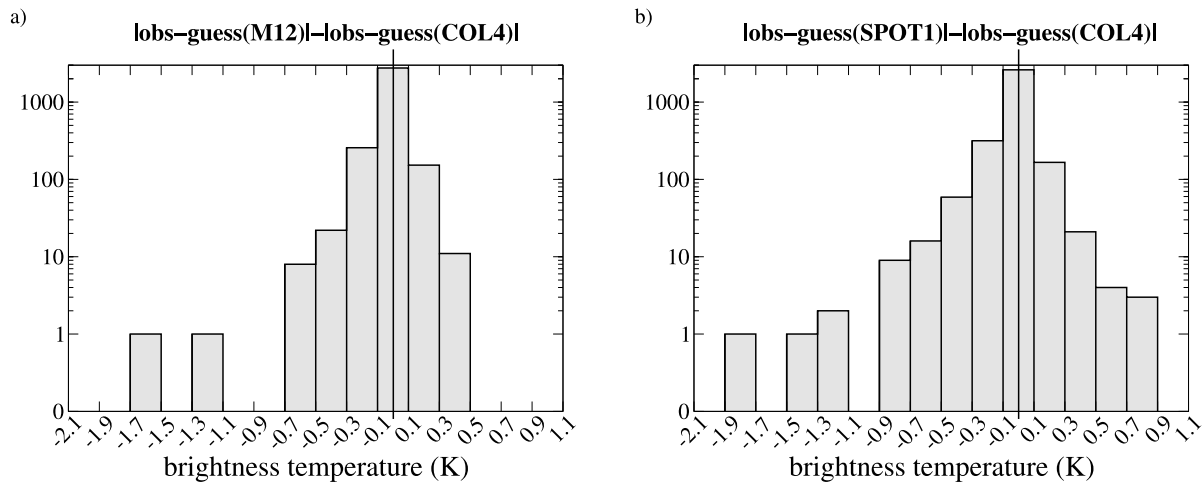**|obs−guess(M12)|−|obs−guess(COL4)|**

b)

|obs−guess(SPOT1)|−|obs−guess(COL4)|

Figure 9. Histograms of the brightness temperature differences between |obs − guess| obtained with a new observation operator, (a) M12 or (b) SPOT1, and |obs − guess| obtained with COL4 for all IASI WV channel 2919 clear observations over the western Mediterranean in September 2007.

2919. There are more negative differences than positive differences, which indicates that SPOT1 and, to a lesser extent, M12 provide model equivalent brightness temperatures more often closer to the observations. This is also true for the other IASI WV channels while, in contrast, for TLW channels, the simulations with the new observation operators are more often slightly further from the observations and, for TSW channels, no clear signal can be found (not shown). Figure 9 also shows that the negative differences are stronger than the positive differences. This is corroborated for all IASI WV channels by Figure 10, which shows some statistics of these differences. This means that the decreases in the observation-guess departures of WV channels with the new observation operators are larger than the increases. The greatest decreases are as large as 1 K to 2.5 K with SPOT1 and 0.5 K to 1.9 K with M12 according to the WV channel con-

sidered. Still, in most cases, these decreases do not reach more than 0.5 K with SPOT1 and 0.25 K with M12. It is interesting to note that the size of the changes in the observation-guess departures does not depend on the magnitude of the initial departure obtained using COL4 (not shown). The improvements in the fit to WV channels are much larger than the degradations of the fit to TLW channels: with both SPOT1 and M12, the increases in the observation-guess departures of TLW channels remain in most cases below 0.04 K and do not reach more than 0.05 K to 0.15 K according to the TLW channel considered. The overall observation-guess biases of TLW channels are consequently only very slightly increased: only by 1% to 4% according to the channel considered (increase of less than 0.005 K for all TLW channels except the near-surface ones for which the increase can reach up to 0.016 K). This is consistent with
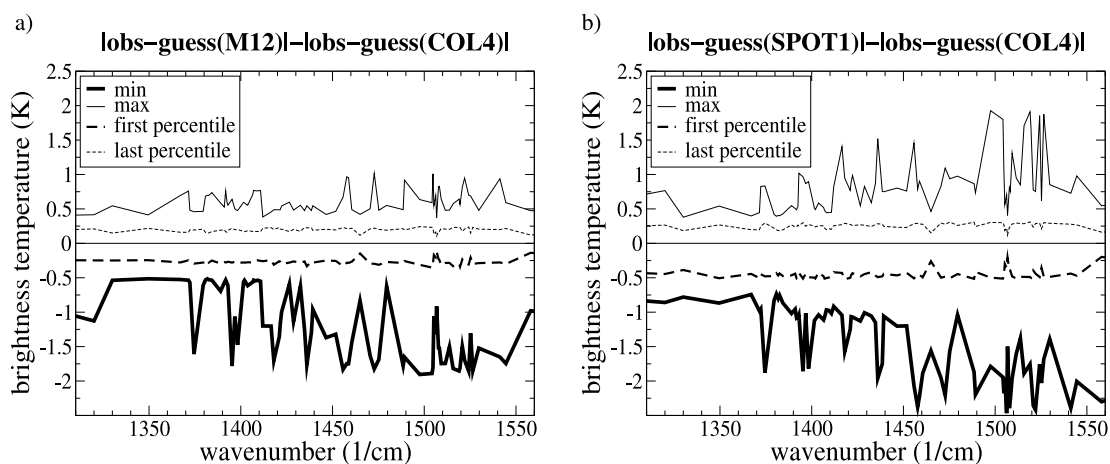
a)

|obs−guess(M12)|−|obs−guess(COL4)|

b)

|obs−guess(SPOT1)|−|obs−guess(COL4)|

Figure 10. Minimum, maximum, first, and last percentiles of the brightness temperature differences between |obs − guess| obtained with a new observation operator, (a) M12 or (b) SPOT1, and |obs − guess| obtained with COL4 for clear IASI observations over western Mediterranean of September 2007 in all the WV channels studied displayed according to increasing wave number along the abscissa.
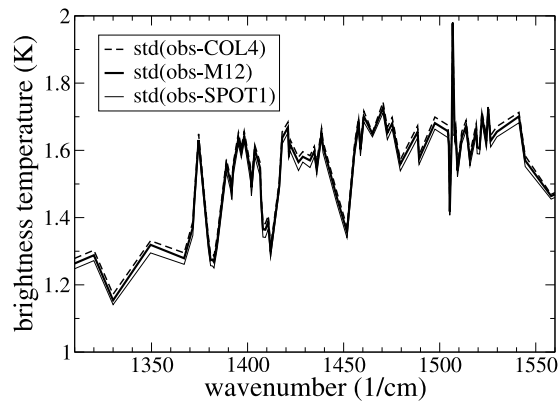
Figure 11. Standard deviation of the brightness temperature differences between observation and guess obtained with COL4, M12, and SPOT1 for clear IASI observations over the western Mediterranean of September 2007 in all the WV channels studied, displayed according to increasing wave number along the abscissa.

the results of section 3.2 showing, for off-nadir observation simulation, that the impact of the new observation operators in TLW channels is most of the time lower than the instrument noise and does not introduce new bias.

[33] Whereas the bias of the observation minus guess departures is almost unchanged in the WV channels (not shown) and very slightly increased in the TLW channels (as stated above), the standard deviation is slightly reduced for both WV and TLW channels (Figure 11 for WV channels) when the simulation is performed with SPOT1 and, to a lesser extent, M12. For TSW channels, these statistics remain mostly unchanged (not shown). All these results show that using the new observation operators should

help to reduce the number of WV channel observations rejected during the assimilation process.

5. Single Observation Assimilation Experiment

5.1. Experiment Setup

[34] The impact of a change in the observation operator formulation is now examined in terms of analysis increment. We determine what impact the differences in the simulation of IASI or AIRS observations identified above may have on the final analysis. To do this, we performed assimilation experiments of a single IASI observation. In these experiments, we assimilated one specific channel of an IASI observation (see Figure 12 a for its location) at 2100 UTC, 6 September 2007. This observation was chosen because it was clear for the cloud-detect software, over the sea and in a region with mesoscale humidity gradients in a relatively dry environment (Figure 12). Quite large differences were thus found between its simulations with the various observation operators. Either a WV or a TLW IASI channel of this observation spot was assimilated. The WV and the TLW channels chosen were the ones having the strongest differences between the new observation operators and COL4: WV channel 3244 or TLW channel 275.

[35] Twin single observation assimilation experiments were performed using COL4 and M12. The differences between these twin experiments are not only their direct observation operator but also their jacobian and adjoint used to compute the analysis increments (model corrections applied to the first guess). With COL4, the elements of the jacobian are the partial derivatives of the brightness temperature with respect to the interpolated model variables whereas with M12, they are the derivatives with respect to the 12-point mean model variables. To assimilate an observation, the COL4 and M12 adjoints use the innovation (observation minus model equivalent simulation) and these
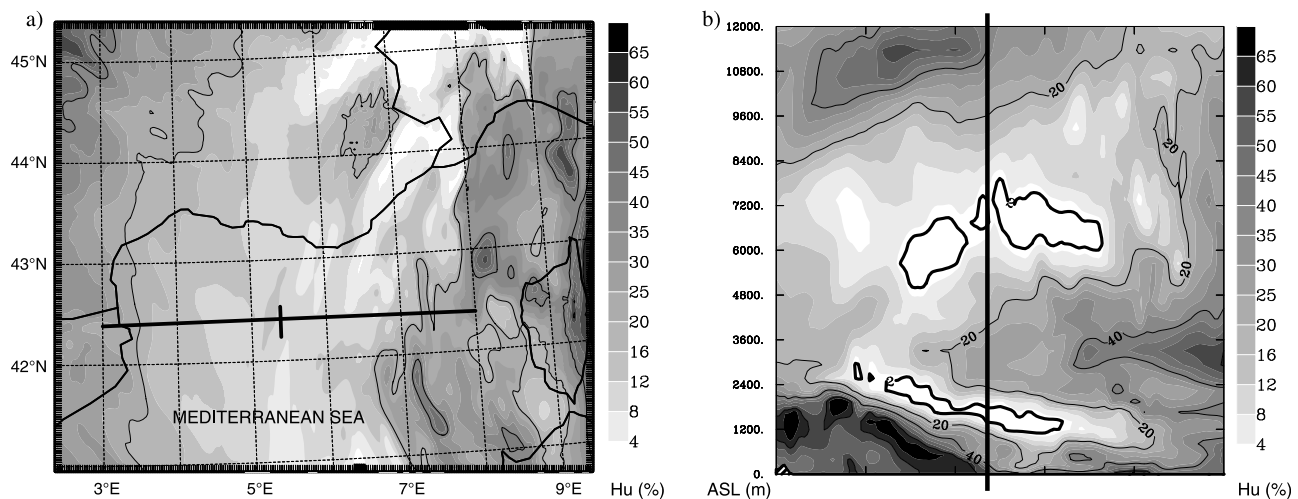

Figure 12. Location of the assimilated IASI observation (a) in the working area with the background relative humidity at 8700 m (grey scale on the right of Figure 12a and contours at 20% and 40%) and (b) in the vertical cross section along the line drawn in Figure 12a of the background relative humidity at 2100 UTC, 6 September 2007 (grey scale on the right of Figure 12b and contours at 2%, 20%, 40%, and 60%). The altitude is given in meters on the left of Figure 12b. The assimilated IASI observation is marked by the vertical line.

Table 3. Departures Between Observation and First Guess or Analysis Obtained With Both COL4 and M12 for the Two Single Observation Assimilation Experiments of IASI Channel 3244 and IASI Channel 275 Observations

		Observation-Guess		Observation-Analysis	
	Observation	COL4	M12	COL4	M12
Channel 3244	241.90 K	2.85 K	2.64 K	0.03 K	0.02 K
Channel 275	241.81 K	1.30 K	1.29 K	0.12 K	0.12 K

single Jacobians to determine the model correction to be applied. They distribute this correction over the four model grid points with weights proportional to their distance to the center of the observation spot or over the 12 model grid points with the same weight. The experiments assimilate a near-nadir observation having an observation spot that covers 18 grid points, so that SPOT1 and M12 are very similar and no additional assimilation experiment was carried out with SPOT1.

5.2. Results

[36] Table 3 gives the departures between the observation and the first guess and between the observation and the analysis for both twin assimilation experiments. As was to be expected according to the results of section 4, it shows that the first guess and the analyses are closer to the observations when the observation operator M12 is used. This is more obvious for channel 3244. According to the statistics over the whole of September 2007 discussed in section 4, using M12 improves the model equivalent estimation in TLW channel 275 by more than 0.012 K and in WV channel 3244 by more than 0.11 K for only about 10% of the observations. The reductions of the observation minus guess departure obtained here are therefore quite substantial with 0.21 K for channel 3244 and 0.012 K for channel 275.

[37] The impact of the observation operator formulation on the humidity and temperature analyses was evaluated. The differences between the analyses using M12 or COL4 were negligible for temperature and for both channels as the maximum difference was less than 0.006 K. Figure 13 displays the differences in terms of relative humidity between the analyses obtained using COL4 and M12 for the two channels. The results are perturbed in the area with less than 2% relative humidity as the drying induced by the assimilation of the observation was limited. Still, the differences are clearly weak, less than 0.4%. These differences result from slightly weaker increments due to smaller observation minus first-guess departures obtained using M12 (see Table 3). Modifying the first-guess error covariance matrix or the observation errors did not modify the conclusion of this study (not shown). All the single observation assimilation experiments performed here show that even the largest differences in the model equivalent estimation obtained using different observation operators have almost no impact on the final analysis of temperature and humidity.

6. Conclusions and Outlook

[38] This study has aimed to evaluate the impact of the observation operator formulation on the model-equivalent simulation for the assimilation of satellite infrared radiances in AROME. In particular, the question of the aggregation of the model information when the model grid mesh is 1 order smaller than the satellite spot has been addressed. Three new observation operators, M12, SPOT1 and SPOT2, have been defined in order to come closer to the way the satellite measurement is achieved. To characterize the sounded atmosphere, they aggregate part or all of the model information contained within the satellite field of view with the same weight instead of using only the single model column
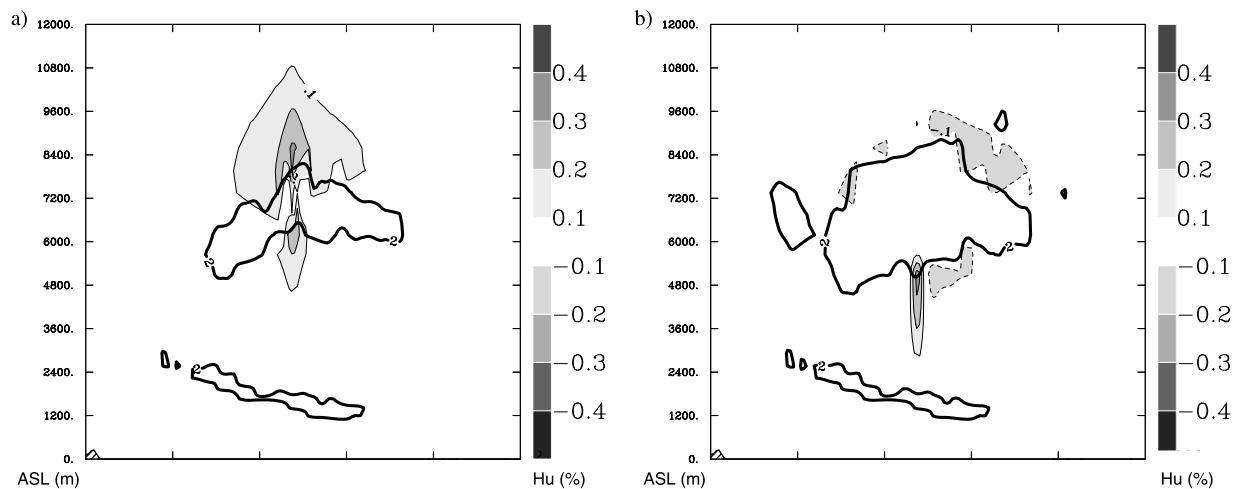

Figure 13. Vertical cross section along the axis drawn in Figure 12a of the differences in relative humidity between the analyses formed by the assimilation with M12 and COL4 (a) of the IASI WV channel 3244 observation and (b) of the IASI TLW channel 275 observation, at 2100 UTC, 6 September 2007. The grey scale in percent is to the right of each plot. Contours delimit the areas with less than 2% relative humidity in the analysis.

situated at the center of the observation spot as is done in the current observation operator (COL4).

[39] A comparison among the four observation operators was made over a 1 month period using the 3-hourly AROME analyses. Substantial differences were found between the various operators for water vapor channels only (peaking under 340 hPa and also above 800 hPa for AIRS) and where fine-scale horizontal humidity gradients occurred in the sounded layer. With the new observation operators, these fine-scale model humidity variations that cannot be measured by the satellite because they have a smaller size than the observation resolution, are filtered out. The greatest differences occur for very dry observed layers. Aggregating model information contained within the satellite spot before (SPOT1) or after (SPOT2) applying the radiative transfer led to no significant differences in most cases. For an operational use, the observation operator that consumes less computing time, SPOT1, can be given preference without substantial loss of accuracy. The M12 operator (aggregating model information over 12 grid points) provided results that are intermediate between SPOT1 and COL4.

[40] The model equivalent observations simulated by the various operators have then been compared to real observations by performing the screening step of the AROME data assimilation cycle. The observation operators were thus applied to the 3 h forecast that served as first guess in the AROME rapid update cycle. The comparison was carried out over a full 1 month period to reduce the weight of the model errors in this comparison. Using the new observation operators proved to reduce (up to 2 K) most of the time the departures between observations and simulations of WV channels while their impact was neutral for TSW and slightly negative for TLW channels. The standard deviation of these departures was slightly reduced for WV channels but also for most TLW ones. These improvements in WV channels were independent of the departure between observation and simulation with COL4. So, aggregating the model information over the whole spot rather than taking only the model information at the center of the satellite spot improves the estimation of the model equivalent observation by filtering out the model fine-scale patterns that are not detected by the satellite because of its lower spatial resolution. A better estimation of the model equivalent observation should lead to fewer observation rejections and reduce incorrect analysis increments due to representativeness errors.

[41] To evaluate the impact of the observation operator formulation in terms of analysis increment, single observation assimilation experiments were performed. Situations and channels having shown the largest differences between the observation operators were selected. They showed, however, that even large differences in the simulation of IASI observations have a negligible impact on the analysis of temperature and relative humidity.

[42] Even though the impact on the analysis increment of the differences between the model equivalent estimations from the various observation operators seems neutral, the modifications of the observation operator may have a larger influence on the whole data assimilation suite (bias correction, cloud detection, selection of assimilated observations, …). Future work will evaluate the overall impact of such modifications of the observation operator on a complete data assimilation cycle. The impact may be enhanced because of cycling and because the modifications of the observation operator affect many elements of the assimilation process, which in turn modify the analysis.

References

Auligné, T., A. P. McNally, and D. Dee (2007), Adaptive bias correction for satellite data in a numerical weather prediction system, *Q. J. R. Meteorol. Soc.*, *133*(624), 631–642.

Aumann, H. H., et al. (2003), AIRS/AMSU/HSB on the Aqua mission: Design, science objectives, data products, and processing systems, *IEEE Trans. Geosci. Remote Sens.*, *41*(2), 253–264.

Berg, W., J. J. Bates, and D. L. Jackson (1999), Analysis of upper-tropospheric water vapor brightness temperatures from SSM/T2, HIRS and GMS-5 VISSR, *J. Appl. Meteorol.*, *38*, 580–595.

Berre, L. (2000), Estimation of synoptic and mesoscale forecast error covariances in a limited area model, *Mon. Weather Rev.*, *128*(3), 644–667.

Blumstein, D. (2005), IASI on METOP: On ground calibration of the FM2 instrument, paper presented at 14th International TOVS Study Conference, VCS, Beijing.

Blumstein, D. (2007), In-flight performance of the infrared atmospheric sounding interferometer (IASI) on METOP-A, *Proc. SPIE Int. Soc. Opt. Eng.*, *6684*, 12 pp., doi:10.1117/12.734162.

Brenot, H., V. Ducrocq, A. Walpersdorf, C. Champollion, and O. Caumont (2006), GPS zenith delay sensitivity evaluated from high-resolution numerical weather prediction simulations of the 8–9 September 2002 flash flood over southeastern France, *J. Geophys. Res.*, *111*, D15105, doi:10.1029/2004JD005726.

Brousseau, P., F. Bouttier, G. Hello, Y. Seity, C. Fischer, L. Berre, T. Montmerle, L. Auger, and S. Malardel (2008), A prototype convective-scale data assimilation system for operation: The AROME-RUC, *Tech. Rep. 68*, EUMETNET, Norrköping, Sweden.

Bubnová, R., G. Hello, P. Bénard and J.-F. Geleyn (1995), Integration of the fully elastic equations cast in the hydrostatic pressure terrain-following coordinate in the framework of the ARPEGE/Aladin NWP system, *Mon. Weather Rev.*, *123*(2), 515–535.

Caumont, O., and V. Ducrocq (2008), What should be considered when simulating Doppler velocities measured by ground-based weather radars?, *J. Appl. Meteorol. Climatol.*, *47*(8), 2256–2262.

Caumont, O., V. Ducrocq, G. Delrieu, M. Gosset, J.-P. Pinty, J.-P. du Châtelet, H. Andrieu, Y. Lemâitre, and G. Scialom (2006), A radar simulator for high-resolution nonhydrostatic models, *J. Atmos. Oceanic Technol.*, *23*(8), 1049–1067.

Cayla, F. (2001), L'interféromètre IASI, un nouveau sondeur satellitaire à haute résolution, *Meteorol. Ser. 8*, *32*, 23–39.

Chalon, G., F. Cayla, and D. Diebel (2001), IASI: An advanced sounder for operational meteorology, paper presented at 52nd Congress, IAF, Toulouse, France.

Collard, A. (2007), Selection of IASI channels for use in numerical weather prediction, *Q. J. R. Meteorol. Soc.*, *133*(629), 1977–1991.

Courtier, P., J.-N. Thépaut, and A. Hollingsworth (1994), A strategy for operational implementation of 4D-Var using an incremental approach, *Q. J. R. Meteorol. Soc.*, *120*(519), 1367–1387.

Dee, D. (2004), Variational bias correction of radiance data in the ECMWF system, paper presented at Workshop on Assimilation of High Spectral Resolution Sounders in NWP, ECMWF, Reading, U. K.

Diebel, D., F. Cayla, and T. Phulpin (1996), IASI mission rationale and requirements, *CNES/EUMETSAT Tech. Rep. IA-SM-0000-10-CNE/EUM–4b*, 35 pp., EUMETSAT, Darmstadt, Germany.

Ducrocq, V., D. Ricard, J.-P. Lafore, and F. Orain (2002), Storm-scale numerical rainfall prediction for five precipitating events over France: On the importance of the initial humidity fields, *Weather Forecasting*, *17*, 1236–1256.

Ducrocq, V., F. Bouttier, S. Malardel, T. Montmerle, and Y. Seity (2005), Le projet AROME, *Houille Blanche*, *2005-2*, 39–43.

Edwards, D. P. (1992), GENLN2: A general line-by-line atmospheric transmittance and radiance model, *NCAR Tech. Note NCAR/TN-367 +STR*, 147 pp., NCAR, Boulder, Colo.

Elliott, D. A., T. S. Pagano, and H. H. Aumann (2006), The impact of AIRS spatial response on channel-to-channel and multi-instrument data analyses, *Proc. SPIE Int. Soc. Opt. Eng.*, *6296*, 30 pp.

Fischer, C., T. Montmerle, L. Berre, L. Auger, and S. E. Stefanescu (2005), An overview of the variational assimilation in the ALADIN/France numerical weather prediction system, *Q. J. R. Meteorol. Soc.*, *131*(613), 3477–3492.

Guidard, V., C. Fischer, M. Nuret, and A. Dziedzic (2006), Evaluation of the ALADIN 3D-Var with observations of the MAP campaign, *Meteorol. Atmos. Phys.*, *92*, 161–173.

Kim, G., and A. P. Barros (2002), Space-time characterization of soil moisture from passive microwave remotely sensed imagery and ancillary data, *Remote Sens. Environ.*, *81*, 393–403.

Kleespies, T. J. (2009), Microwave radiative transfer at the sub-field-of-view resolution, paper presented at 16th International TOVS Study Conference, Petrobras, Angra dos Reis, Brazil.

Lafore, J.-P., et al. (1998), The Meso-NH Atmospheric Simulation System. Part I: Adiabatic formulation and control simulations, *Ann. Geophys.*, *16*, 90–109.

McNally, A. P., and P. D. Watts (2003), A cloud detection algorithm for high-spectral resolution infrared sounders, *Q. J. R. Meteorol. Soc.*, *129*(595), 3411–3423.

Merlin, O., A. G. Chehbouni, Y. H. Kerr, E. G. Njoku, and D. Entekhabi (2005), A combined modeling and multi-spectral/multi-resolution remote sensing approach for disaggregation of surface soil moisture: Application to SMOS configuration, *IEEE Trans. Geosci. Remote Sens.*, *43*(9), 2036–2050.

Nuissier, O., V. Ducrocq, D. Ricard, C. Lebeaupin, and S. Anquetin (2008), A numerical study of three catastrophic precipitating events over western Mediterranean region (southern France). Part I: Numerical framework and synoptic ingredients, *Q. J. R. Meteorol. Soc.*, *134*(630), 111–130.

Pagano, T. S., H. H. Aumann, S. L. Gaiser, and D. T. Gregorich (2002), Early calibration results from the Atmospheric InfraRed Sounder (AIRS) on Aqua, *Proc. SPIE Int. Soc. Opt. Eng.*, *4891*, 76–83.

Pagano, T. S., H. H. Aumann, D. E. Hagan, and K. Overoye (2003), Prelaunch and in-flight radiometric calibration of the Atmospheric InfraRed Sounder (AIRS), *IEEE Trans. Geosci. Remote Sens.*, *41*(2), 265–273.

Radnóti, G., et al. (1995), The spectral limited area model ARPEGE-ALADIN, *WMO TD 699*, pp. 111–118, WMO, Geneva.

Reichle, R., D. Enthekabi, and D.B. McLauglin (2001), Downscaling of radio brightness measurements for soil moisture estimation: A four-dimensional variational data assimilation approach, *Water Resour. Res.*, *37*(9), 2353-2364, doi:10.1029/2001WR000475.

Saunders, R., and P. Brunel (2005), RTTOV_8_7 user's guide, *NWPSAF-MO-UD-008*, 45 pp., EUMETSAT, Darmstadt, Germany.

Soden, B. J., and F. P. Bretherton (1996), Interpretation of TOVS water vapor radiances in terms of layer-average relative humidities: Method and climatology for the upper, middle and lower troposphere, *J. Geophys. Res.*, *101*(D5), 9333–9343.

Susskind, J., C. D. Barnet, and J. M. Blaisdell (2003), Retrieval of atmospheric and surface parameters from AIRS/AMSU/HSB data in the presence of clouds, *IEEE Trans. Geosci. Remote Sens.*, *41*(2), 390–409.

Yan, X., V. Ducrocq, G. Jaubert, P. Brousseau, P. Poli, C. Champollion, C. Flamant, and K. Boniface (2009), The benefit of GPS zenith delay assimilation to high-resolution quantitative precipitation forecasts: A case-study from COPS IOP 9, *Q. J. R. Meteorol. Soc.*, *135*(644), 1788–1800, doi:10.1002/qj.508.

V. Ducrocq, F. Duffourg, and G. Jaubert, Groupe de Météorologie de Moyenne Echelle, Centre National de Recherches Météorologiques, Météo-France, 42 av. Gaspard Coriolis, F-31057 Toulouse CEDEX 1, France. (fanny.duffourg@meteo.fr)

N. Fourrié and V. Guidard, Groupe de Modélisation pour l'Assimilation et la Prévision, Centre National de Recherches Météorologiques, Météo-France, 42 av. Gaspard Coriolis, F-31057 Toulouse CEDEX 1, France.